

Review

Numerical Simulation of Heat and Mass Transfer Behavior during Iron Ore Sintering: A Review

Zhengjian Liu ¹, Zhen Li ¹, Yaozu Wang ^{2,3,*}, Jianliang Zhang ^{1,*}, Jiabao Wang ¹, Lele Niu ¹, Sida Li ¹ and Ben Feng ¹

- ¹ School of Metallurgical and Ecological Engineering, University of Science and Technology Beijing, 30th Xueyuan Road, Haidian District, Beijing 100083, China; liuzhengjian@ustb.edu.cn (Z.L.); m202210224@xs.ustb.edu.cn (Z.L.); m202110242@xs.ustb.edu.cn (J.W.); b20200136@xs.ustb.edu.cn (L.N.); d202210144@xs.ustb.edu.cn (S.L.); m202110204@xs.ustb.edu.cn (B.F.)
- ² School of Intelligence Science and Technology, University of Science and Technology Beijing, 30th Xueyuan Road, Haidian District, Beijing 100083, China
- ³ Institute of Artificial Intelligence, University of Science and Technology Beijing, 30th Xueyuan Road, Haidian District, Beijing 100083, China
- * Correspondence: yaozuwang@ustb.edu.cn (Y.W.); zhang.jianliang@hotmail.com (J.Z.)

Abstract: Accurate computational models of sintering behavior would assist to enhance sinter quality and are anticipated to play a role in yield prediction. Sintering is a vital process in the manufacturing of iron and steel. As a consequence, the primary objective of these models will be a thorough simulation of mass and heat transport during the sintering process. In this paper, based on the examination and integration of previous studies, the fundamental physical formula and chemical reactions of the numerical simulation of the sintering process are introduced in depth with mechanism analysis. Furthermore, in view of the current numerical simulation methods and sintering process technology innovation development, the studies on sintering numerical simulation are reviewed from different angles, of which the main methods and assumptions are discussed. Finally, the current state of sintering simulation including the numerical simulation of innovative algorithm and optimized sintering technology is discussed in detail, along with potential implications for model development.

Keywords: ironmaking; sintering behavior; simulation; CFD modeling



Citation: Liu, Z.; Li, Z.; Wang, Y.; Zhang, J.; Wang, J.; Niu, L.; Li, S.; Feng, B. Numerical Simulation of Heat and Mass Transfer Behavior during Iron Ore Sintering: A Review. *Metals* **2023**, *13*, 1277. <https://doi.org/10.3390/met13071277>

Academic Editor: Hong Yong Sohn

Received: 29 June 2023

Revised: 12 July 2023

Accepted: 14 July 2023

Published: 15 July 2023



Copyright: © 2023 by the authors. Licensee MDPI, Basel, Switzerland. This article is an open access article distributed under the terms and conditions of the Creative Commons Attribution (CC BY) license (<https://creativecommons.org/licenses/by/4.0/>).

1. Introduction

Iron ore sintering refers to the process of mixing iron ore, fuel, flux, and iron-containing waste produced in the ironmaking and steelmaking process in a certain proportion, and then the fuel is burned through ignition to release heat. Some particles of the mixture are softened or melted by physical and chemical reactions between various raw materials, resulting in a certain liquid phase and infiltrating other solid particles. Finally, after cooling, the particles are bonded into blocks. The sintering process is one of the key technologies to ensure the smooth progress of blast furnace ironmaking. At present, the most widely used sintering production method all over the world is negative pressure suction sintering. As shown in Figure 1, the negative pressure suction sintering process adds the sintering mixture to the sintering pallet after granulation. The sintering pallet moves along a certain track to the discharge place and ignites on the mixture surface through the ignition area, making fuel in the mixture begin to burn. The above is the beginning of the sintering reaction. At the same time, negative pressure suction air boxes are set under the sintering pallet. The high-temperature sintering flue gas gradually heats the mixture through the sintering material layer and continuously ignites the fuel in the mixture from the surface of the material layer downward, as shown in the longitudinal section of the sintering material layer in Figure 1 [1–3]. The sintering mixture is subjected to a series of physical and chemical changes during high-temperature combustion and cooling processes to generate sinter [4].

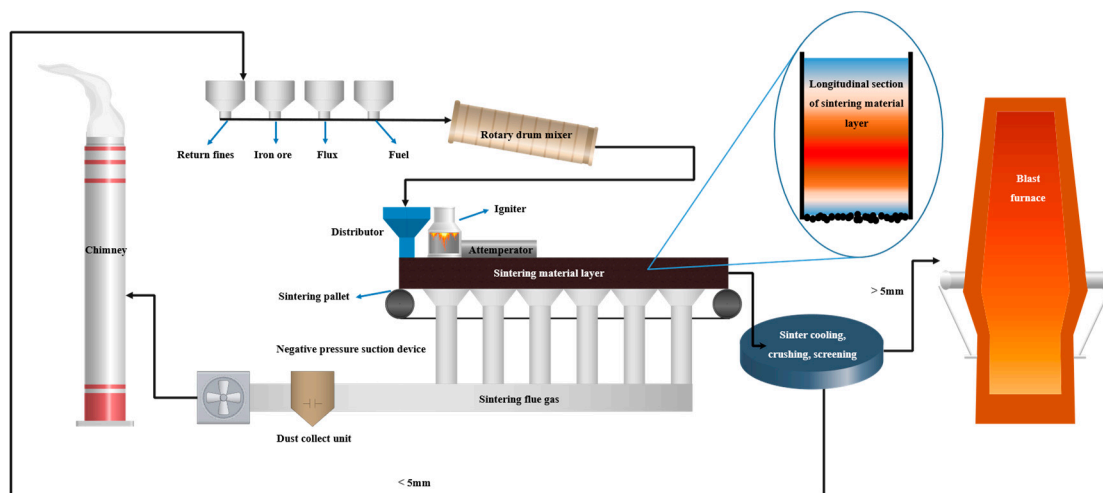


Figure 1. Iron ore sintering process diagram.

Researchers and software designers are both researching sintering modeling and simulation. The board's goals are to properly predict part qualities and performance and to effectively convey the importance of each process parameter [5]. Reliable models are suggested to be crucial in process certification and yield prediction, in addition to helping to choose the parameters for improving sinter quality. The longer-term goal is to use simulation-based techniques and information from process diagnostics to actively regulate the sinter manufacturing process [6–8].

Other sub-models, such as those that represent the burning of coke and reduction and oxidation of iron oxide, can be used to simulate various parts of the sintering process. The overall goal is to integrate the sub-models in the process of numerical simulation into a “multi-scale” simulation of the sintering process that, in conjunction with knowledge of the relationships between material, temperature, and property, forecasts process qualification and yield prediction for given process parameters.

In the last several years, a number of helpful evaluations of sintering modeling and simulation have been released. Park et al. [9] divided the sintering process into drying zone, sintering zone, and cooling zone and discussed to efficiently acquire critical data such as temperature distribution, humidity, and iron oxide mass fraction in the sintering process by establishing computational fluid dynamics (CFD) models. In addition, the authors also briefly introduced the differences in using different modeling and simulation software. However, the research focuses on the analysis of the role of the sintering process modeling and simulation in promoting the progress of sintering, while the physical and chemical reactions and simulation methods of the sintering process are not fully explained. Yan et al. [10] systematically reviewed the numerical simulation of the data-driven sintering process and evaluated the current published research models from the perspectives of process prediction, control, and optimization. This study is of great significance for improving the prediction accuracy of sintering process parameters based on deep learning modeling methods and optimizing the stability of numerical simulation. Cheng et al. [4] reviewed the sustainable energy-saving technology of sintering production, which includes some research on the prediction of sintering process parameters based on numerical simulation model. The research shows that using a numerical simulation model to predict the quality of sintered minerals and explore the parameters such as solid fuel segregation is of great significance for sintering heat balance. While this review mainly analyzes the progress of experimental technology, the research progress of numerical simulation is still not comprehensive enough.

With two objectives that set it apart from earlier papers, this study primarily focuses on the simulation of sintering behavior and models of the sintering process. Firstly, the major chemical reaction rates of the sintering process must be compiled in formula form by

carefully examining the fundamental physical formulas used in the numerical modeling of the sintering process and behavior. The second is to provide an overview of the development process of sintering simulation works more thoroughly and precisely than previous review studies and evaluate different simulation methods and critically analyze different treatment methods for important influencing factors in the sintering process in previous studies, such as boundary conditions, material properties of the sintering layer, physical and chemical changes, and so on [11]. We anticipate that researchers who are establishing numerical simulation models of sintering processes could find valuable information in this paper.

In Section 2, the basic physical theoretical equations of the model are introduced in detail. In Section 3, the formula and calculation method of sintering process reaction are described in detail. Section 4 summarizes the work status of the published research, and discusses the current research status, research significance, and development direction of the model. Conclusions are presented in Section 5.

2. Sintering Simulation Theory

The sintering mixture enters the stable sintering stage following ignition and heat preservation, based on the process's numerical simulation model. There are intricate physical and chemical interactions during the entire process. In the height direction, heat and mass transfer are continuous, but at a particular stage of the sintering process, the motion of heat and mass in a vertical dimension of the material layer exhibits stratification-like features.

The sintering process has been simulated using a number of different calculation techniques. However, they all essentially require solving the same fundamental physical equations, and the formulae employed in the various models change only in detail. The formulas in the subsequent chapters are written with CFD in consideration. The CFD numerical simulation methodology is the most typical approach for numerically modeling flow and the sintering process.

2.1. Simulation Requirements

The main requirements of the sintering model are as follows:

- (1). Visually represent the temperature distribution of the sintering layer.
- (2). Analyze the causes of each phenomenon in the sintering process.
- (3). Reflect the change of pressure drop caused by physical and chemical changes during sintering.
- (4). Reflect the whole process of sintering reaction by model operation to make people understand the sintering behavior and mechanism better.

The simulation comprises a linked fluid flow and heat transfer problem that takes into account the following physical effects:

- (1). The sintering process includes not only gas–gas reaction but also gas–solid multiphase reaction, such as coke combustion, reduction, and oxidation of iron oxides.
- (2). The heat of ignition is transferred from the superstratum of the material to the bottom. Due to the large specific heat capacity of the sintering mixture, there is a self-heat storage phenomenon in the sintering process; furthermore, the maximum temperature of the lower mixture increases, and the holding time is prolonged.
- (3). Because the mixture contains moisture, the process involves evaporation and condensation.
- (4). The phase transition of the material would happen accompanied by a heating and cooling process, such as melting and solidification, which is accompanied by the absorption and release of latent heat.
- (5). The flow of gas in the sintering material layer will be affected by the permeability of the material layer.
- (6). The sintering process involves complex heat transfer forms such as radiation, conduction, and convection.

2.2. Fundamental Physical Equations

Based on previous research results, it can be seen that it is necessary to simplify the CFD model of the sintering process as follows:

- (1). Both gas and solid phases of sintering material are homogenous and continuum.
- (2). The mathematical model is based on using partial differential equations to solve mass, momentum, and energy conservations.
- (3). The sintering materials is represented as a porous material, resulting in laminar or turbulent fluid flow.

The gas phase's continuity is denoted by [12,13]

$$\frac{\partial(\varepsilon\rho_g)}{\partial t} + \vec{\nabla} \cdot (\varepsilon\rho_g \vec{V}) = SOURCE_{mass-s} + SOURCE_{mass-g} \quad (1)$$

Each species' gas transfer equation is solved to get the concentration of gaseous species [14]:

$$\frac{\partial(\rho_g \varepsilon Y_i)}{\partial t} + (\vec{V} \cdot \vec{\nabla})(\rho_g Y_i) = \vec{\nabla} \cdot (\rho_g \varepsilon D_i \vec{\nabla} Y_i) + SOURCE_i \quad (2)$$

In Equation (2), the source term represents the rate of reactions of the i -th gaseous species. In general, homogeneous gas phase processes and heterogeneous gas–solid interactions are responsible for the reactions.

The solid phase's continuity is denoted by [12,13]

$$\frac{\partial((1-\varepsilon)\rho_s)}{\partial t} = -SOURCE_{mass-s} \quad (3)$$

The following is the general form of momentum equations for incompressible flow in a porous medium [15–17]:

$$\frac{\partial(\rho_g \vec{V})}{\partial t} + (\vec{V} \cdot \vec{\nabla})(\rho_g \vec{V}) = -\vec{\nabla} P + \vec{\nabla} \cdot (\mu \vec{\nabla}) \vec{V} - SOURCE_{momentum} \quad (4)$$

Because the temperature of the gas and solid phases varies rapidly with time, the presumption of thermal equilibrium between gas and solid is unavailable. As a result, the gas phase energy equation should be solved using the two-medium method, as shown below [14]:

$$\frac{\partial(\rho_g \varepsilon C_{Pg} T_g)}{\partial t} + \vec{\nabla} \cdot (\rho_g \vec{V} C_{Pg} T_g) = \vec{\nabla} \cdot \left[(K_{g,eff} + \rho_g \varepsilon C_{Pg} D_t) \vec{\nabla} T_g \right] + SOURCE_g \quad (5)$$

It is possible to formulate the solid phase energy equation as [14,18]

$$\frac{\partial(\rho_s (1-\varepsilon) C_{Ps} T_s)}{\partial t} = \vec{\nabla} \cdot \left[(K_{s,eff} + K_r) \vec{\nabla} T_s \right] + SOURCE_s \quad (6)$$

The other material properties are usually temperature-dependent but directly expressed except heat transfer parameters such as thermal conductivity which will be reviewed in Section 2.5.

2.3. Additional Momentum Source Terms

The additional momentum contributions denoted by $SOURCE_{momentum}$ in Equation (4) are explored in this section.

The material will generate a resistance proportionate to the speed of the gas in the material layer because the impact of sintering material on the gas flow is dealt by the porous

medium while modeling. Therefore, the model must be modified to include a momentum source term with a corrective effect. $SOURCE_{momentum}$ consists of two parts: the viscous loss term and the inertial loss term, as follows [19–22]:

$$SOURCE_{momentum} = \frac{\mu}{\alpha} \vec{V} + \frac{1}{2} C_2 \rho_g \left| \vec{V} \right| \vec{V} \quad (7)$$

The viscous resistance coefficient $\frac{1}{\alpha}$ and inertial resistance coefficient C_2 are calculated using the modified Ergun equation, which is usually described as [23]

$$\frac{1}{\alpha} = \frac{150\mu X^2(1-\varepsilon)^2}{\varepsilon^3 D_p^2} \quad (8)$$

$$C_2 = \frac{3.5X(1-\varepsilon)}{\varepsilon^3 D_p^2} \quad (9)$$

2.4. Additional Heat Transfer Source Terms

The remaining terms $SOURCE_g$ and $SOURCE_s$ in Equations (5) and (6) reflect further contributions to heat transport, and these contributions are examined in this section.

$SOURCE_g$ represents the heat generated by gas homogeneous combustion, the heat of gas–solid convection heat transfer, the heat of gas–solid radiation heat transfer, the heat of gas–solid heterogeneous reaction which enters the gas phase, and the enthalpies of gas generated by gas–solid heterogeneous reaction, which usually is expressed as follows [24,25]:

$$SOURCE_g = S_{conv} + S_{rad,sg} + S_g + S_S + S_{sg} \quad (10)$$

$SOURCE_s$ includes the heat of gas–solid convection heat transfer, the heat of gas–solid radiation heat transfer, the enthalpies of gas generated by gas–solid heterogeneous reaction, the heat of gas–solid reaction entering the solid phase, and the heat changes generated by the solid phase melting or solidification process, as shown [26–28]:

$$SOURCE_s = -S_{conv} - S_{rad,sg} - S_S + S_{SS} - S_m \quad (11)$$

2.4.1. Gas–Solid Convection Heat Transfer

The heat generated by convective heat transfer is generally considered in the model [29]:

$$S_{conv} = h \cdot A_s (T_s - T_g) \quad (12)$$

This is related to the Nusselt number of a single particle $Nu = 2 + 0.75(Re)^{0.5}(Pr)^{0.33}$, since most of the scholars believe that the sintering layer is a packed bed model and porous medium. The Nu of multiple particles is modified, which will be discussed in Section 2.5.

2.4.2. Gas–Solid Radiative Heat Transfer

Generally, the efficiency of gas–solid radiative heat transfer is higher than that of convective heat transfer, as shown below [30]:

$$S_{rad,sg} = \sigma \varepsilon A_s (T_s^4 - T_g^4) \quad (13)$$

In the formula, ε is generally calculated by the following blackness formula of radiation heat transfer system [31]:

$$\varepsilon = \frac{1}{\frac{1}{\varepsilon_s} + \frac{1}{\varepsilon_g} - 1} \quad (14)$$

2.4.3. Heat Generated by Homogeneous Gas Combustion

Gas phase reactions such as combustible gas combustion will produce heat absorption and release phenomena. The expression is as follows [32,33]:

$$S_g = \sum_j R_j H_j \quad (15)$$

2.4.4. Enthalpy of Entrained Gas Generated by Gas–Solid Heterogeneous Reaction

When gas–solid phase reaction produces gas, it is usually accompanied by heat conversion because of the entrained gas enthalpy [34]:

$$S_s = C_{Pg} T_g \sum_k M_k H_k \quad (16)$$

2.4.5. Heat of Gas–Solid Heterogeneous Reaction Transfer to Gas Phase

The gas–solid heterogeneous reaction is accompanied by the consumption and generation of heat. Part of the heat is distributed to the solid phase, and the other part is distributed to the gas phase, resulting in a change in the heat of the gas phase [35]:

$$S_{sg} = (1 - \alpha) \sum_k R_k H_k \quad (17)$$

2.4.6. Heat of Gas–Solid Heterogeneous Reaction Transfer to Solid Phase

The gas–solid heterogeneous reaction is accompanied by the consumption and generation of heat. Part of the heat is distributed to the solid phase, resulting in a change in the heat of the solid phase:

$$S_{ss} = \alpha \sum_k R_k H_k \quad (18)$$

2.4.7. Solid Phase Melting and Solidification Processes

Since the sintering process is a high-temperature process, there are often melting and solidification phenomena of solid phase materials. The endothermic or exothermic process will affect the energy of solid phase materials [36]:

$$S_m = (1 - \varepsilon) \rho_s \frac{\partial f}{\partial T_s} \frac{\partial T_s}{\partial t} H_m \quad (19)$$

2.5. Coefficient of Gas–Solid Volumetric Convective Heat Transfer

The current research shows that the gas–solid convection heat transfer is the most important heat transfer mode in the sintering process, so the selection and determination of the heat transfer coefficient plays a decisive role in the stable and accurate operation of the calculation. Most scholars calculate the gas–solid convection heat transfer coefficient through the Nusselt numerical empirical formula and the modified model h_v [37]:

$$h_v = \frac{6h(1 - \varepsilon)}{D_p} \quad (20)$$

Most scholars believe that h should be defined in this way [38]:

$$Nu = \frac{h D_p}{\lambda_g} \quad (21)$$

The modified formula is shown in Table 1:

Table 1. The modified Nu of porous medium.

Expressions	Researchers
$\varepsilon Nu = 2 + 0.75(Re)^{\frac{1}{2}}(Pr)^{\frac{1}{3}}$	I. Muchi et al. [39]
$Nu = 2 + 0.6(Re)^{\frac{1}{2}}(Pr)^{\frac{1}{3}}$	N. K. Nath et al. [40,41]
$Nu = 2 + 1.1(Re)^{0.6}(Pr)^{0.33}$	Won. Yang et al. [42]
$Nu = 2 + 0.39(Re)^{0.5}(Pr)^{0.33}$	J. A. de Castro et al. [43,44]
$Nu = 7.48 + 0.25(Re)^{1.32}(Pr)^{-1.1}$	A. Aissa et al. [45]

3. Chemical Reactions

The chemical reactions in the sintering process should be divided into multiphase reactions and homogeneous reactions [14]. This chapter comprehensively summarizes the important chemical reaction sub-models published in advanced research in recent years, hoping to provide help for CFD modeling and simulation researchers.

3.1. Homogeneous Reactions

The gas phase reactions considered in different sintering simulation models are quite different. At present, the gas phase reactions considered in the sintering model are developing in a comprehensive and accurate direction. The reactions and their chemical reaction rates are shown in Table 2 [46,47].

Table 2. Rate of homogeneous reactions.

Reactions	Rate (mol/m ³ ·s)
$2CO_{(g)} + O_{2(g)} = 2CO_{2(g)}$	$1.3e8C_{O_2}^{0.5}C_{CO_2}^{0.5}C_{CO}exp\left(-\frac{15,100}{T_g}\right)$
$CO_{(g)} + H_2O_{(g)} = H_{(g)} + CO_{2(g)}$	$2.78C_{CO}C_{H_2O}exp\left(-\frac{1510}{T_g}\right)$
$2H_{2(g)} + O_{2(g)} = 2H_2O_{(g)}$	$10^{11}C_{H_2}C_{O_2}exp\left(-\frac{5050}{T_g}\right)$
$H_{2(g)} + CO_{2(g)} = CO_{(g)} + H_2O_{(g)}$	$93.96C_{CO_2}C_{H_2}exp\left(-\frac{5604}{T_g}\right)$
$CH_{4(g)} + 2O_{2(g)} = CO_{2(g)} + 2H_2O_{(g)}$	$9.2e6C_{CH_4}^{0.5}C_{O_2}exp\left(-\frac{9622}{T_g}\right)$
$2CO_{2(g)} = 2CO_{(g)} + O_{2(g)}$	$7.5e11C_{CO_2}exp\left(-\frac{46,500}{T_g}\right)$

3.2. Heterogeneous Reactions

3.2.1. Coke Combustion

An essential exothermic step in the sintering process is the burning of coke. Coke may react with oxygen, carbon dioxide, and water vapor as reactants. These types of reactions would take place on the surface of particles. In order to initiate a chemical reaction, gas must first adsorb to the surface of the particles after passing through the ash layer and gas film boundary layer around the coke carbon particles [14], as shown in Figure 2. Therefore, the following assumptions are required for the derivation of the coke combustion reaction rate equation:

- (1). The coke particles exhibit a spherical structure.
- (2). There is no secondary reaction between coke carbon particles and inside coke.
- (3). Gas–solid heterogeneous reaction occurs between coke and gas reactants.
- (4). The contact of coke does not affect the boundary layer of surrounding particles.
- (5). The occurrence of each reaction follows the characteristics of chemical reaction kinetics.
- (6). The combustion degree of coke is inversely proportional to the effective mass transfer coefficient of ash layer.
- (7). The resistance to diffusion in the burning of coke is comprised of the resistance of the ash layer, the resistance of the material wrapped outside the particles, and the resistance of the boundary layer.

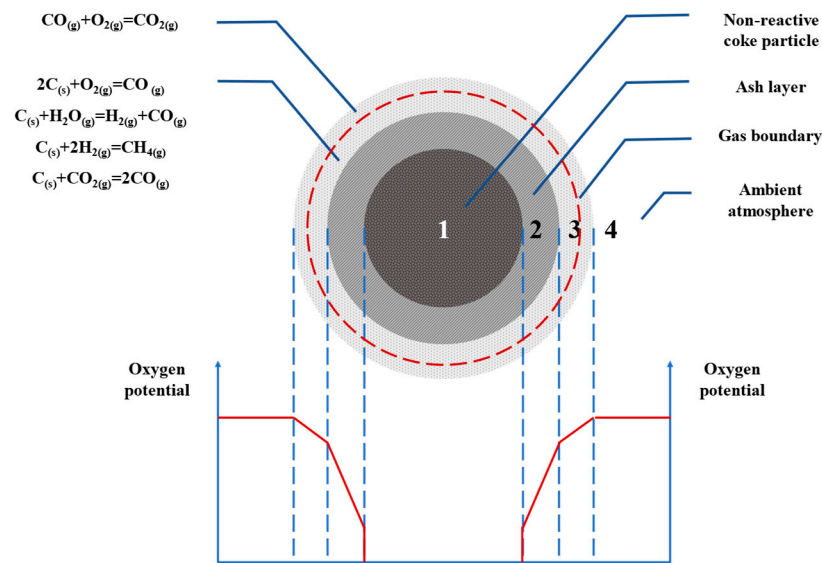


Figure 2. Coke combustion reaction model and oxygen potential distribution.

Based on the assumptions made above, the reaction rate of coke combustion may be computed using the formula below [48]:

$$R_k = \frac{A_p n_c C_i}{\frac{1}{\xi K_{r,c,i}} + \frac{1}{K_{g,i}} + \frac{1}{K_{eff,i}}} \quad \& \quad i = \text{O}_2, \text{H}_2\text{O}, \text{H}_2, \text{CO}_2 \quad (22)$$

$$K_{eff,i} = \frac{(1 - G)D_p}{2D_{eff,i}} \quad (23)$$

Table 3 shows the reaction kinetic rate constants of the above reactions [14,49,50].

Table 3. Reaction kinetic rate constants.

Reactions	Rate (mol/m ³ ·s)
$2\text{C}_{(s)} + \text{O}_{2(g)} = 2\text{CO}_{(g)}$	$K_{r,c,\text{O}_2} = 1.715T_s \exp\left(-\frac{9000}{T_s}\right)$
$\text{C}_{(s)} + \text{H}_2\text{O}_{(g)} = \text{H}_{2(g)} + \text{CO}_{(g)}$	$K_{r,c,\text{H}_2\text{O}} = 3.42T_s \exp\left(-\frac{15,600}{T_s}\right)$
$\text{C}_{(s)} + 2\text{H}_{2(g)} = \text{CH}_{4(g)}$	$K_{r,c,\text{H}_2} = 3.42e - 3T_s \exp\left(-\frac{15,600}{T_s}\right)$
$\text{C}_{(s)} + \text{CO}_{2(g)} = 2\text{CO}_{(g)}$	$K_{r,c,\text{CO}_2} = 589T_s \exp\left(-\frac{26,800}{T_s}\right)$

3.2.2. Reduction of Iron Oxides

In the preheating zone and combustion zone of the sintering material layer, due to the presence of reducing gases such as CO and H₂, the reduction reaction processes of iron oxide may occur based on thermodynamic conditions. The process is an endothermic process. In the published reaction model, the three-stage reduction process of Fe₂O₃ → Fe₃O₄ → FeO → Fe is considered to be the most reasonable reduction process. When the material layer temperature is higher than 570 °C, the reduction reaction could occur. The process follows the gas–solid unreacted core model, as shown in Figure 3.

The reaction rate of iron oxides reduction can be calculated as follows [51,52]:

$$R_k = A_p \frac{\rho_g}{W} \sum_k \alpha_k \left(K_k \frac{Y_{\text{CO}_{or}\text{H}_2}}{M_{\text{CO}_{or}\text{H}_2}} - \frac{Y_{\text{CO}_{2or}\text{H}_2}}{M_{\text{CO}_{2or}\text{H}_2}} \right) \quad (24)$$

$$K_{\text{CO}-1} = \exp\left(7.255 + \frac{3720}{T_s}\right) \quad (25)$$

$$K_{CO-2} = \exp\left(5.289 - \frac{4711}{T_s}\right) \quad (26)$$

$$K_{CO-3} = \exp\left(-3.127 - \frac{2879}{T_s}\right) \quad (27)$$

$$K_{H_2-1} = \exp\left(10.32 + \frac{362}{T_s}\right) \quad (28)$$

$$K_{H_2-2} = \exp\left(8.98 - \frac{8580}{T_s}\right) \quad (29)$$

$$K_{H_2-3} = \exp\left(1.30 - \frac{2070}{T_s}\right) \quad (30)$$

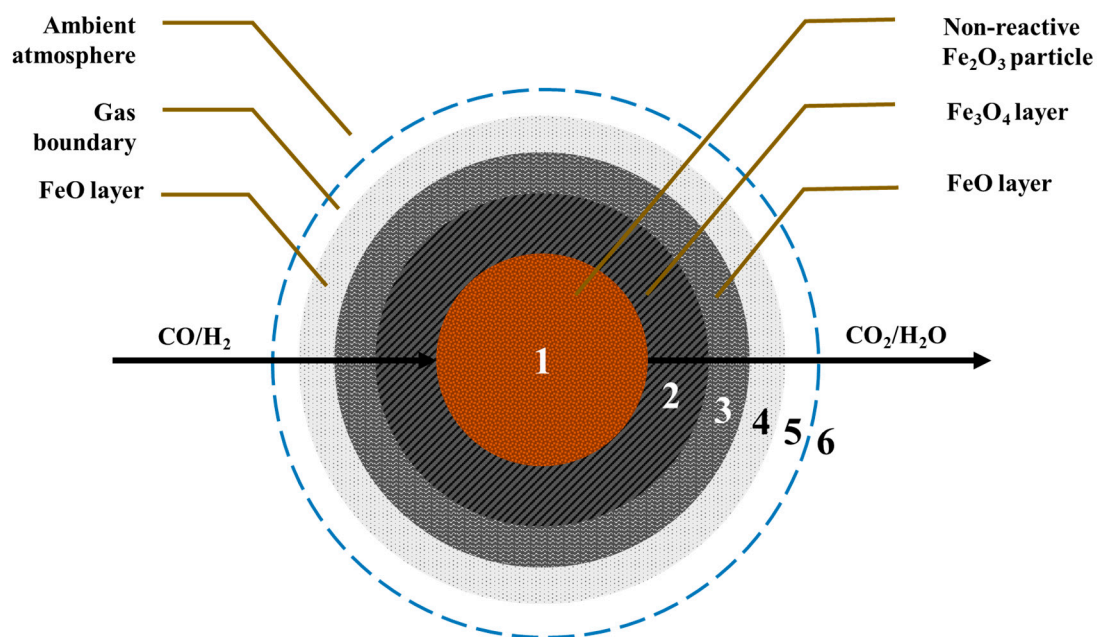


Figure 3. Iron oxides reduction model.

3.2.3. Oxidation of Iron Oxides

When magnetite is included in the sintering mixture, the effect of magnetite's oxidation reaction process on the temperature field and gas products of the sintering bed must be taken into account. Magnetite undergoes an exothermic oxidation process, and gas boundary layer diffusion and product layer diffusion regulate the rate of the reaction. The reaction shows a trend of ring-inward advancement, and the single-interface unreacted core model is generally used to characterize the oxidation kinetics of magnetite [32].

$$R_k = \frac{n_{Fe_3O_4} 4\pi r_0^2 (C_{O_2} - C_{O_2}^*)}{\frac{1}{k_{O_2}} \left(\frac{r}{r_0}\right)^2 + \frac{r_0(r_0-r)}{r D_{eff,O_2}} + \frac{1}{K_{g,O_2}}} \quad (31)$$

$$C_{O_2}^* = \frac{101,325.0 K_{O_2}}{8.314 \times 10^3 T_s} \quad (32)$$

$$K_{O_2} = \exp\left(40.69 - \frac{70,649.22}{T_s}\right) \quad (33)$$

$$k_{O_2} = 3.0 \times 10^2 \exp\left(-\frac{6000}{T_s}\right) \tag{34}$$

3.2.4. Water Evaporation and Condensation

Undried water found in the ore, flux, and fuel, water added during the mixture’s granulation, traces of water introduced into the atmosphere, water produced during the combustion of hydrocarbons, and water produced by the decomposition of minerals in the mixture are the main sources of moisture in the sintering material layer.

The mass transfer rate of the gas boundary layer or the difference between the particle surface saturated vapor pressure $P_{saturation}$ and the gas vapor pressure P_{H_2O} , must first be calculated before the moisture drying rate [53].

$$P_{saturation} = \exp\left(25.541 - \frac{5211}{T_s}\right) \tag{35}$$

$$K_{g,H_2O} = \frac{hT_g}{3.155P\sqrt{(1 - 0.24X_m)\left(1 + \frac{X_m}{7}\right)(1 - X_m)}} \tag{36}$$

The molar proportion of vapor and the saturated contact surface is represented by X_m [54].

$$r_R = \frac{A_s K_{g,H_2O}}{8.314T_g} (P_{saturation} - P_{H_2O}) \tag{37}$$

The evaporation and condensation rate of water r_R is related to solid moisture content w_s , and critical moisture content w_c is shown in Table 4 [55,56].

Table 4. The evaporation and condensation rate.

Judging Condition	Rate (mol/m ³ ·s)
$r_R < 0$	$R_{cond} = r_R$
$r_R > 0$ & $w_s > w_c$	$R_{evp} = r_R$
$r_R > 0$ & $w_s < w_c$	$R_{evp} = r_R \left(1 - \left(1 - \frac{w_s}{w_c}\right) \times \left(1 - 1.796\frac{w_s}{w_c} + 1.059\left(\frac{w_s}{w_c}\right)^2\right)\right)$

3.2.5. Carbonate Decomposition Reaction

Carbonate in the material layer may often be entirely disintegrated during the sintering process at high temperatures. CaCO₃ and dolomite make up the majority of the carbonate in the sintered combination, and the breakdown reaction is endothermic. At 720 °C, CaCO₃ started to break down, and at 880 °C, it achieved the chemical boiling sintering state. It can be known that the reaction was essentially not constrained by diffusion factors, and the reaction rate was mostly influenced by temperature since CO₂ was simple to spread during the reaction due to the modest external diffusion barrier [57].

$$R_k = \frac{n_{CaCO_3} 4\pi r^2 (C_{CO_2}^* - C_{CO_2})}{\frac{C_{CO_2}^*}{k_{CO_2}} \left(\frac{r_0}{r}\right)^2 + \frac{r_0(r_0-r)}{rD_{eff,CO_2}} + \frac{1}{K_{g,CO_2}}} \tag{38}$$

$$k_{CO_2} = 1.52 \times 10^6 \exp\left(-\frac{20,134.4}{T_s}\right) \tag{39}$$

$$C_{CO_2}^* = \frac{K_{CO_2}}{8.314 \times 10^3 T_s} \tag{40}$$

$$K_{CO_2} = 101,325 \exp\left(7.0099 - \frac{8202.5}{T_s}\right) \tag{41}$$

Dolomite is one of the most important flux in sintering raw materials whose decomposition reaction products are CaO, MgO, and CO₂. The reaction rate is as follows:

$$R_k = 1.67 \times 10^7 \exp\left(-\frac{1.9067 \times 10^5}{8.314T_s}\right) \left(\frac{r}{r_0}\right)^{0.4043} \quad (42)$$

4. Summary of Published Research

This section summarizes the published research in the area of sintering simulation. The development path of the technology is evaluated, as shown in Figure 4, along with the benefits and drawbacks of various approaches.

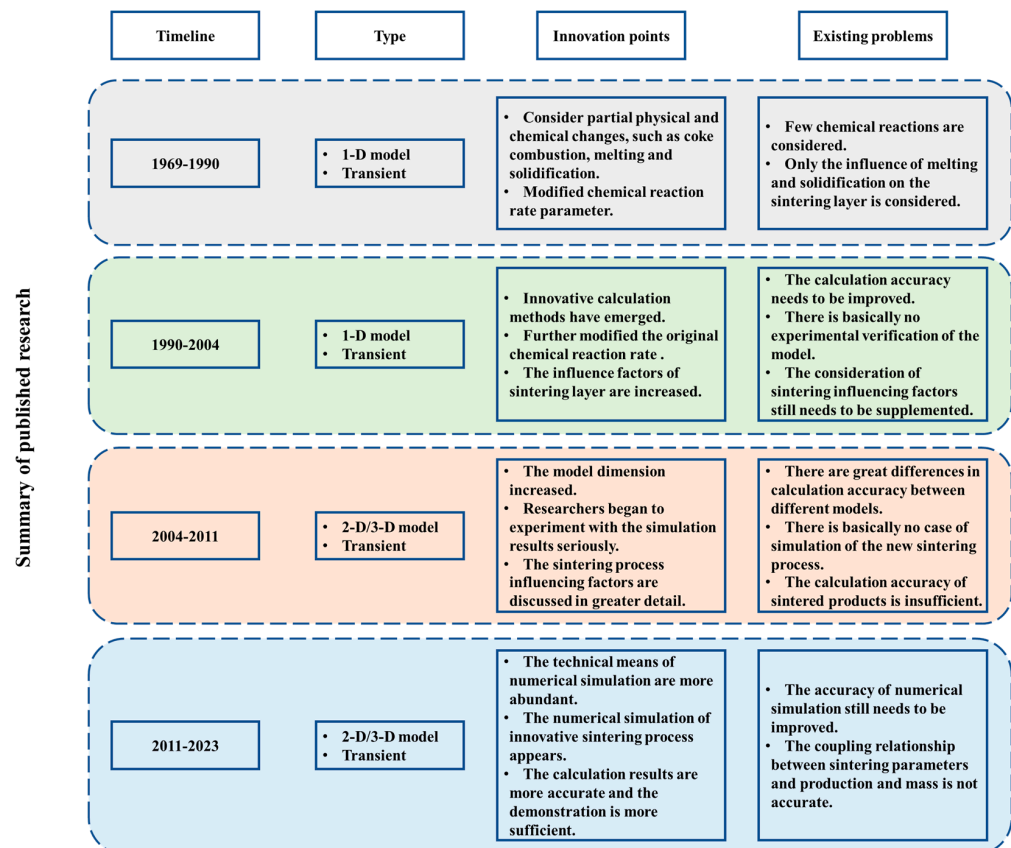


Figure 4. Schematic diagram of the development path of sintering numerical simulation.

4.1. Simulation of Temperature Distribution in Sintering Process

In the early stage of the development of sintering numerical simulation technology, T. Tukamoto et al. [58,59] established a mathematical model including coke combustion, water evaporation, limestone decomposition, and iron ore melting and solidification. The solid phase and gas phase properties of the sintering process change with temperature, and the chemical reaction rate of the above reaction is expressed. Through the above research, the transient numerical simulation of the sintering process can be realized and the relevant data in the sintering process can be detected.

I. Muchi et al. [39,60,61] established the heat transfer and reaction rate equations from the perspective of the effective heat transfer area changing with time, the effective distribution coefficient, and diffusion coefficient under the condition of solid-liquid coexistence in the sintering process and verified the accuracy through experiments. This study is conducive to optimizing the accuracy of the numerical simulation model of the sintering process. In addition, they used partial differential equations to establish a numerical simulation of the sintering process considering coke combustion, water evaporation, and the reaction rate following the unreacted core model. However, as shown in Table 5, the

number of chemical reactions considered in the model is small, and the chemical reaction rate still needs to be corrected and optimized, resulting in a large deviation between the numerical simulation results and the actual production.

Table 5. Summary of publications of temperature distribution.

Basic Equation	Method	Reaction	Result
<ul style="list-style-type: none"> • Effective heat exchange area • Distribution coefficient under the condition of solid-liquid coexistence • Chemical reaction rate 	<ul style="list-style-type: none"> • Solving partial differential equations • Difference method • Special curve method 	<ul style="list-style-type: none"> • $C_{(s)} + O_{2(g)} = CO_{2(g)}$ • $H_2O_{(l)} \rightleftharpoons H_2O_{(g)}$ • $CaCO_{3(s)} = CaO_{(s)} + CO_{2(g)}$ 	<ul style="list-style-type: none"> • Sintering layer temperature distribution

Y. Liu et al. [62] established a numerical simulation model of sintering process based on sintering waste heat utilization technology, and the simulation of heat flow such as heat transfer was mainly carried out. Researchers ignored the chemical reaction of the sintering process but explained the energy transfer process of the sintering process in detail. In this paper, there are more detailed data detection and result analysis, and the calculation method used in the model is helpful to shorten the calculation time.

With more in-depth research, Y. Liu et al. [41] conducted numerical simulation prediction and experimental research on the heat transfer of the random packed bed in the sintering process. In this study, the parameter formula of the heat transfer coefficient was updated and corrected. This study is of great significance for the calibration of the *Nu* coefficient in the subsequent numerical simulation of the sintering process. At the same time, the accuracy of the numerical simulation results was verified by experiments. According to the standard error, the accuracy of the numerical simulation calculation became better.

4.2. Simulation Considering Actual Production Parameters and Product Properties

H. Toda et al. [63] established a sintering process simulation model considering the particle size distribution of coke powder, water condensation reaction, iron oxide formation, iron oxide reoxidation reaction, and other reactions. The relationship between temperature change and sinter quality in the sintering process was studied in detail. In addition, the effects of temperature distribution and material properties on the properties of sintering products were investigated through experiments.

E. Kasai et al. [64] established a method to measure the pressure drop and temperature in the bed based on the actual sintering mixture ratio. Considering the changes in porosity and particle size in the sintering process and the changes in permeability caused by ore melting and solidification, the pressure drop in the bed was numerically simulated. More chemical reactions are designed in the model, and the accuracy of the model results is verified through experiments.

T. Kawaguchi et al. [65] established an integrated numerical simulation model of sintering process considering six sub-models, namely magnetite oxidation, temperature change, raw material melting process, porosity, mineralization, and quality prediction model. The model takes industrial parameters as the initial conditions and supplements more comprehensive sintering production data, which can predict energy consumption, sinter quality, and output in the sintering process.

The key chemical processes in the mathematical model of the sintering process created by L. Jianming et al. [66] are the decomposition of limestone, the burning of coke, the evaporation of water, and the condensation of water. The model mainly considers the distribution of each zone and the change of temperature field in the sintering process based on these two conditions. The model can change the physical conditions of the sintering mixture to calculate the air volume distribution, the distribution of each zone in the material layer, and the temperature field in the material layer.

N. K. Nath et al. [40] established a transient numerical simulation model of sintering process. The model made several predictions about the sintering process, such as the temperature of the gas phase and solid phase, the concentration of different materials, the quantity of solid melting, etc. In this model, the accuracy of various predictive variables is verified by experimental values. However, the simulation results shown in this study have some deviations from the simulation results in other future studies, which may be caused by the accuracy of the chemical reaction rate expression.

H. Yamaoka and T. Kawaguchi established a three-dimensional numerical simulation model of the sintering process [67,68]. The temperature change and chemical composition change of the sintering layer can be accurately predicted. However, the chemical reaction in the study is still not comprehensive enough, and the rationality of the chemical rate needs to be improved.

B. Zhang et al. [69] established a numerical simulation model of the sintering process to predict sinter yield and strength. This study primarily aims to investigate the impact of heat and carbon concentration on the yield and robustness of the sintering process. The novelty of this study lies in its establishment of a correlation between cooling rate and sinter strength and indirect discussion of the correlation between the coke content and sinter strength via cooling rate. In addition, this paper uses two-layer sintering as a method of heat supplement in the sintering process. A summary is presented in Table 6.

Table 6. Summary of publications considering actual parameters and product properties.

Basic Equation	Method	Reaction	Result
<ul style="list-style-type: none"> • Pressure drop equation • Mass conservation equation • Energy conservation equation • Chemical reaction rate 	<ul style="list-style-type: none"> • Solving partial differential equations • Establish mathematical models based on computer language • Experimental verification 	<ul style="list-style-type: none"> • $C_{(s)} + O_{2(g)} = CO_{2(g)}$ • $H_2O_{(l)} \rightleftharpoons H_2O_{(g)}$ • $CaCO_{3(s)} = CaO_{(s)} + CO_{2(g)}$ • Solid \rightleftharpoons Liquid • $Fe_2O_{3(s)} \rightleftharpoons Fe_3O_{4(s)} \rightleftharpoons FeO_{(s)} \rightleftharpoons Fe_{(s)}$ • $CO_{2(g)} + C_{(s)} = 2CO_{(g)}$ • $C_{(s)} + H_2O_{(g)} = H_2_{(g)} + CO_{(g)}$ 	<ul style="list-style-type: none"> • Sintering layer temperature and pressure drop distribution • Properties of sintering products • Sintering flue gas composition • Chemical composition changing of sintering layer

4.3. Simulation of Influencing Factors of Sintering Process Parameters

J. Mitterlehner et al. [70] established a numerical simulation model of sintering process considering gas–solid multiphase flow and carbon monoxide oxidation, coke combustion, sintering material melting and solidification, limestone decomposition, and other processes. This study believes that the heat transfer front will have a greater impact on the sintering process. The accuracy of the numerical simulation results is verified through the sintering cup experiment. The results show that the average diameter of the particles in the packed bed, the porosity in the packed bed, the amount of coke powder added, the humidity of the sintering mixture, and the Fe_2O_3 content in the ore are the main influencing factors of the heat transfer front.

W. Yang et al. [71] established a numerical simulation model of the sintering process containing a variety of solid-phase structures. A variety of solid-phase structures were achieved by adjusting the material properties of each sintering mixture. In the model calculation process, thermal radiation and heat conduction were considered. At the same time, the simulation of bed shrinkage was added to the model. The bed shrinkage was mainly achieved by reducing the particle size. Experiments were used to confirm that the findings of the model calculations were accurate. The innovation of this study lies in the richer characterization of the model simulation results, the introduction of the bed shrinkage calculation, the detailed analysis of the heat transfer process, and the more

detailed description of the physical parameters of the sintered mixture. However, the bed shrinkage method of the process needs to be optimized.

X. Zhang et al. [72] established a numerical simulation model of the sintering cooling process, which is mainly used to calculate the waste heat recovery and optimization technology in the cooling process. This study mainly investigated the influence of sinter particle size, inlet gas velocity and temperature, and porosity and height of the sinter layer on sintering waste heat recovery and calculated the most influential parameters as the main influencing factors.

J. Zhao et al. [34] established a combustion model for the sintering process. This study conducted a detailed analysis of the combustion behavior of coke during the sintering process, which is of great significance for analyzing the combustion behavior of sintering, and the combustion behavior of coke and its influencing factors have a great influence on the sintering flame front. The numerical simulation model not only describes the details of coke combustion but also describes the heat transfer behavior when the flame front passes through the sintered material layer. Therefore, this study has a promoting effect on the use of gas fuel as a heat supplement source for some coke.

H. Zhou et al. [73–75] carried out CFD calculation and analysis of the pressure drop and effective thermal conductivity of the sintering bed based on the porous medium structure. In this study, the real pore structure in the sintering bed was reproduced based on X-ray microtomography. Based on this structure, the non-uniform gas flow mode in the structure can be further explored. The study shows that the pore structure of the sintering bed has a great influence on the pressure drop of the sintering process, which can affect the flame front of the sintering process. However, the sintered material layer in the study takes a smaller structure of $30 \times 30 \times 30 \text{ mm}^3$, which has a certain gap with the real sintered material.

B. Zhang et al. [76] established a mathematical model to describe the particle growth in the sintering process of iron ore. In this study, not only can the model calculate and predict the temperature change in the sintering process, but it can also describe the contour change of the sintering mixture to describe the particle growth process. On this basis, combined with experimental verification, the relationship between solid phase temperature, sintering time, and sintering yield can be predicted and verified through numerical simulation. However, the temperature change cloud diagram shown in this article is slightly inconsistent. There is no explanation of the heat transfer conditions of the container wall, which may be caused by the container properties.

E.A. Gauna et al. [77,78] carried out numerical simulations of heat transfer in the cooling process of porous metal materials. This study obtained the influence of gas flow and pore size on heat transfer and elaborated the specific heat transfer equation, which is of great significance for heat transfer in the sintering process. However, in this study, it is considered that the pore size has little effect on the heat transfer coefficient, and the heat transfer coefficient mainly depends on the gas flow rate. The publications are summarized in Table 7.

4.4. Simulation of Optimized Sintering Technology

G. Wang et al. [32] established a numerical simulation model of the sintering process combined with flue gas recirculation technology. It has a more comprehensive chemical reaction. In terms of heat exchange, convective heat transfer and heat conduction are considered, and the bed shrinkage process is reflected in the simulation process. The bed shrinkage process is reflected by the change in shrinkage rate parameters. This study has the innovation of models and processes.

J. Feng et al. [79] established a numerical simulation model of gas–solid heat transfer process in a sintering waste heat recovery device. This study mainly discusses the influence factors of the cooling process such as air volume, sinter particle size, sintering cup diameter, and sintering cup height on the quality of sinter. It is found that the above parameters have a great influence on the sinter temperature. In addition, the gas–solid heat transfer

expression is modified, which is of great significance to the optimization of gas–solid multiphase flow heat transfer parameters.

Table 7. Summary of publications considering influencing factors of process parameters.

Basic Equation	Method	Reaction	Result
<ul style="list-style-type: none"> • Pressure drop equation • Continuum equation • Mass conservation equation • Energy conservation equation • Chemical reaction rate 	<ul style="list-style-type: none"> • Computational fluid dynamics • Finite difference method • Finite element method • Finite volume method • Experimental verification 	<ul style="list-style-type: none"> • $C_{(s)} + O_{2(g)} = CO_{2(g)}$ • $2C_{(s)} + O_{2(g)} = 2CO_{(g)}$ • $H_2O_{(l)} \rightleftharpoons H_2O_{(g)}$ • $CaCO_{3(s)} = CaO_{(s)} + CO_{2(g)}$ • Solid \rightleftharpoons Liquid • $Fe_2O_{3(s)} \rightleftharpoons Fe_3O_{4(s)} \rightleftharpoons FeO_{(s)} \rightleftharpoons Fe_{(s)}$ • $CO_{2(g)} + C_{(s)} = 2CO_{(g)}$ • $CO_{(g)} + O_{2(g)} = CO_{2(g)}$ • $C_{(s)} + H_2O_{(g)} = H_2(g) + CO_{(g)}$ 	<ul style="list-style-type: none"> • Influencing factors of flame front • Influencing factors of heat transfer • Influence factors of pressure drop and gas velocity • Influencing factors of particle size
..			

Z. Cheng et al. [80–82] established a numerical simulation model of the sintering process, which was used to calculate and optimize the heat distribution of the sintering process by injecting gas fuel and using infrared temperature measurement imaging technology to increase the model's accuracy significantly. This study explores the experimental conditions of various hydrogen-rich gases and points out that the main reason for its optimization is that hydrogen-rich gas combustion can form a secondary combustion zone, and the conclusion is experimentally verified. Its innovation lies in the use of experimental and computational methods to demonstrate that injecting natural gas can reduce the use of solid fuels. Furthermore, they developed multiphase and multicomponent mathematical models for sintering by combining heat and mass transfer, phase transition, and chemical reactions in porous media. The calculation model is used to calculate the effects of gas fuel injection on temperature distribution, combustion efficiency, and combustion zone reaction kinetics. The innovation of this study is mainly to inject gas fuel in the traditional sintering process and to explore the influence of gas fuel on the sintering process.

X. Huang et al. [83] extended the gas fuel type to hydrogen-rich gas and recorded the evolution of microstructure and mineral composition of sinter under hydrogen-rich gas injection. This study combines experimental and simulation results, but the simulation results are quite different from the simulation results of other studies, and its accuracy needs to be further determined.

N. Tsioutsios et al. [84] established a numerical simulation model of sintering process based on gas injection, which focused on simulating the development of the flame front. In this study, the numerical expression of heat transfer coefficient is described in detail, mainly considering the combustion reaction of coke. The innovation of this study is to explore the heat supplement effect of natural gas injection on less coke. The specific research method is to compare the temperature of sintered material layer under the condition of injecting natural gas and not injecting natural gas after reducing the amount of coke. It is concluded that natural gas injection can supplement heat and improve the moving speed of flame front. The above studies are summarized in Table 8.

4.5. Simulation of Innovative Algorithm

N. K. Nath et al. [85] established a numerical simulation model of sintering process based on CFD, genetic algorithm, and double-layer sintering technology. In this study, a complex chemical reaction process was included. The purpose of reducing the coke ratio was achieved by dividing the sintered material layer into the upper layer with normal coke content and the lower layer with reduced coke content. At the same time, the model was mainly established based on the CFD method. Following the completion of the calculations, a genetic algorithm was used to determine the parameters' ideal values, which improved

the sintering process’s efficiency. The creation of the CFD model is thoroughly covered in this paper. The study approach, which is extremely creative and offers a solution for multi-objective optimization of the sintering process, combines a genetic algorithm to improve the parameters.

Table 8. Summary of publications of optimized sintering technology.

Basic Equation	Method	Reaction	Result
<ul style="list-style-type: none"> • Pressure drop equation • Continuum equation • Mass conservation equation • Energy conservation equation • Chemical reaction rate 	<ul style="list-style-type: none"> • Computational fluid dynamics • Finite difference method • Finite element method • Finite volume method • Experimental verification 	<ul style="list-style-type: none"> • $CH_{4(g)} + 2O_{2(g)} = CO_{2(g)} + 2H_2O_{(g)}$ • $C_{(s)} + O_{2(g)} = CO_{2(g)}$ • $2C_{(s)} + O_{2(g)} = 2CO_{(g)}$ • $H_2O_{(l)} \rightleftharpoons H_2O_{(g)}$ • $CaCO_{3(s)} = CaO_{(s)} + CO_{2(g)}$ • Solid \rightleftharpoons Liquid • $Fe_2O_{3(s)} \rightleftharpoons Fe_3O_{4(s)} \rightleftharpoons FeO_{(s)} \rightleftharpoons Fe_{(s)}$ • $CO_{2(g)} + C_{(s)} = 2CO_{(g)}$ • $CO_{(g)} + O_{2(g)} = CO_{2(g)}$ • $C_{(s)} + H_2O_{(g)} = H_2_{(g)} + CO_{(g)}$ 	<ul style="list-style-type: none"> • Effect of sintering optimization method on sintering process parameters and properties of sintered products
..			

B. K. Giri et al. [86,87] established a numerical simulation model of sintering process by genetic algorithm. The process is mainly based on the energy and mass balance of gas phase and solid phase. The process variable parameters of the model are optimized by a genetic algorithm. Finally, the accuracy of the model is verified by experiments, and the accuracy of the model prediction temperature is high.

V Maximiano et al. [88,89] used discrete element method (DEM) to construct a numerical simulation model of bed structure change in the sintering process. In this study, the heat transfer between gas phase and solid phase and the chemical reaction rate of main reactions are the main influencing factors of the heat transfer front in the sintering process. At the same time, the influence of coke addition on bed structure was studied, and the consolidation effect was explained. The main research method of this study is DEM, which is different from the CFD method. The discrete element method can clearly show the change of mixture particles during sintering. The above studies are summarized in Table 9.

Table 9. Summary of publications of innovative algorithm.

Basic Equation	Method	Reaction	Result
<ul style="list-style-type: none"> • Pressure drop equation • Continuum equation • Mass conservation equation • Energy conservation equation • Chemical reaction rate 	<ul style="list-style-type: none"> • Computational fluid dynamics • Discrete Element Method • Deep learning algorithm 	<ul style="list-style-type: none"> • $C_{(s)} + O_{2(g)} = CO_{2(g)}$ • $2C_{(s)} + O_{2(g)} = 2CO_{(g)}$ • $H_2O_{(l)} \rightleftharpoons H_2O_{(g)}$ • $CaCO_{3(s)} = CaO_{(s)} + CO_{2(g)}$ • $Fe_2O_{3(s)} \rightleftharpoons Fe_3O_{4(s)} \rightleftharpoons FeO_{(s)} \rightleftharpoons Fe_{(s)}$ • $CO_{2(g)} + C_{(s)} = 2CO_{(g)}$ • $CO_{(g)} + O_{2(g)} = CO_{2(g)}$ 	<ul style="list-style-type: none"> • Using innovative algorithms to predict sintering process parameters and product properties.
..			

4.6. Discussion

The benefits of numerical simulation should not be ignored, which is essential for advancing sintering production. The following are the primary causes of the aforementioned issues:

- (1) Although certain process variables are ignored, they would not significantly impact the sintering simulation results since they are not the major variables influencing the outcomes [11].
- (2) The significance of production factors to the sintering process and how they affect sintering production could be comprehended by analyzing the sensitivity of each model parameter.
- (3) Although the sintering production value cannot be precisely approximated, the results' proper trend is extremely important for predicting low-cost manufacturing. The capacity to objectively display production patterns also has a guiding value that cannot be overlooked for process optimization, and a perfectly accurate forecast is not always required.

Although the numerical simulation of the sintering process is progressing quickly, the published study still has several significant issues that need to be further investigated.

In terms of model setting:

- (1) It is particularly unfavorable for the assessment and debate of the model's correctness since there is no clear criterion for determining it or discussion of whether the running state of the model converges in the published study.
- (2) In regard to ignoring the quality of meshing, as we all know, mesh quality is of tremendous relevance in the process of model operation. Grid size, grid quality, and other characteristics are critical criteria for researchers to test and recreate the model.

Considering from the process:

- (1) In the current study, most of the researchers have simplified the thermal boundary conditions of the model. Typically, the wall is set as an adiabatic wall, ignoring the heat dissipation caused by the heat conduction of the wall—that is, the side wall effect.
- (2) The particle size of the mixture has only been covered in a few number of published studies when paired with the DEM method. The sintered mixed particles are typically described in published works as single-sized, spherical particles. The sintered mixture's particle size distribution, however, has a considerable impact on the sintering behavior in the actual manufacturing process. As a result, it is important to emphasize how particle size distribution affects sintering behavior.
- (3) In sintering production, fuel segregation is an inevitable phenomenon and has a significant impact on the sintering behavior, which is related to the quality of sinter and the accuracy of simulation calculations of sintering flue gas composition. However, almost no research has been performed to discuss and study the fuel segregation behavior in the sintering process.
- (4) In the study of sintering numerical modeling, the phenomena of sintering air leakage are widely ignored. Nonetheless, sintering workers are eager to find a solution to the issue of sintering air leakage since it is such a significant issue. The development of airflow distribution during the sintering process, as well as the start and end of each reaction in the sintering bed, are significantly impacted by the phenomena of sintering air leakage.
- (5) Just about a quarter of researchers have examined and calculated the material layer shrinkage in the sintering process in relation to the phenomena of material layer shrinkage thus far, and it is challenging to confirm the accuracy of the calculation. The permeability of the sintering bed, one of the key parameters impacting sintering production, will be impacted by the shrinkage of the sintering bed, though, from the standpoint of sintering production. Thus, it is important to include sintering bed shrinkage in future studies.

In the published research on sintering process simulation, there are two main trends over time and technology development:

- (1) Research on publications is growing in quantity and velocity. Since 2010, researchers in the fields of computer, mechanical manufacturing, and energy environment have studied the numerical simulation of the sintering process in addition to the numerical

simulation of sintering that has been done in the direction of metallurgy and chemical industry. The diversity and accuracy of numerical simulation techniques for the sintering process and sintering behavior have substantially increased as a result of interdisciplinary research, which is also a sign of the robust development of numerical simulation models.

- (2) Numerical simulation of the sintering process is playing a more and more important guiding role in industrial production as the verification process gets better and better. At the early stages of the development of sintering numerical simulation, only qualitative analysis can be done since the findings of numerical simulation cannot be replicated and cannot be verified by tests for a variety of reasons. As simulation technology has advanced, researchers have used a variety of experimental techniques, such as sintering cup experiments, to validate the simulation results. They have also simulated different sintering bed behaviors, which is crucial for the future success of real-time prediction by integrating numerical simulation into manufacturing processes.

5. Conclusions

In this review, we discuss the basic physical formulations of the numerical simulation calculations of sintering processes and the development of this field in detail, as well as the important research significance of numerical simulation of sintering processes as an efficient simulation method. Numerical simulation of the sintering process is an important means to study various behaviors and phenomena of the sintering process from the perspective of mechanism. The numerical simulation of sintering behavior can not only predict the sintering layer temperature and various sintering products but also realize the controllable adjustment of raw materials and operation system by changing parameters. These advantages are crucial in the sintering field.

With the development and progress of numerical simulation process of the sintering process, people have developed a more comprehensive and perfect numerical simulation model, which has a great role in promoting the progress of the sintering field, but there are still some problems to be solved. These problems are mainly caused by the complexity of the sintering process and the high computational cost. Therefore, some parameters are often blurred and approximated. In addition, important issues such as the particle size distribution of the sintering mixture and fuel segregation need to be considered by researchers in the future to further optimize the sintering model.

Overcoming the problems and challenges in the current model is of great significance for the further development of the model and guiding the production practice.

Author Contributions: Z.L. (Zhengjian Liu): clear research ideas, finalization, data analysis; Z.L. (Zhen Li): writing articles, data analysis, collecting data; Y.W.: research design, finalization, data analysis; J.Z.: data analysis, research design; J.W.: research design, data analysis; L.N.: data collection, providing ideas; S.L.: data collection, providing ideas; B.F.: data collection, data analysis. All authors have read and agreed to the published version of the manuscript.

Funding: This research was funded by the National Natural Science Foundation of China (52174291), the Beijing New-star Plan of Science and Technology (Z211100002121115), the Central Universities Foundation of China (06500170), the Guangdong Basic & Applied Basic Research Fund Joint Regional Funds-Youth Foundation Projects (2020A1515111008), and the China Postdoctoral Science Foundation (2021M690369).

Data Availability Statement: Data available on request from the authors.

Acknowledgments: The authors gratefully acknowledge the financial support provided by the National Natural Science Foundation of China (52174291), the Beijing New-star Plan of Science and Technology (Z211100002121115), the Central Universities Foundation of China (06500170), the Guangdong Basic & Applied Basic Research Fund Joint Regional Funds-Youth Foundation Projects (2020A1515111008), and the China Postdoctoral Science Foundation (2021M690369).

Conflicts of Interest: The authors declare no conflict of interest.

Nomenclature

A_s (m^2/m^3)	specific surface area of particle
A_p (m^2)	external surface area
C_{Pg} ($\text{J}/\text{kg}\cdot\text{K}$)	specific heat capacity of gas
C_{Ps} ($\text{J}/\text{kg}\cdot\text{K}$)	specific heat capacity of solid
C_i (kmol/m^3)	gas concentration
C_i^* (kmol/m^3)	gas equilibrium concentration
$D_{eff,i}$ (m^2/s)	effective diffusivity coefficient of i -th gaseous species
D_i (m^2/s)	diffusion coefficient of i -th gaseous species
D_p (m)	diameter of particle
D_t (m)	thermal dissipation coefficient
f	the fraction of heat during melting or solidification
G	percentage of the original carbon
h ($\text{W}/\text{m}^2\cdot\text{K}$)	coefficient of convective heat transfer
H_j (W)	heat generated by the j -th gas–gas reaction
H_k (W)	heat generated by the k -th gas–solid reaction
H_m (W)	heat generated by melting and solidification processes
M_k (kg/mol)	molar mass of solid phase components in the k -th gas–solid reaction
Nu	Nusselt number
M_i (kg/mol)	molar mass of gaseous species in the i -th gas–solid reaction
n	particle count per unit volume
k	chemical reaction number
$K_{eff,i}$ (m/s)	i -th gaseous species' effective mass transfer coefficient in the ash layer
$K_{g,eff}$ ($\text{W}/\text{m}\cdot\text{K}$)	effective thermal conductivity in the gas phase
$K_{g,i}$ (m/s)	i -th gaseous species volume mass transfer coefficient via gas film
K_r ($\text{W}/\text{m}\cdot\text{K}$)	radiation thermal conductivity equivalent
$K_{r,c,i}$ (m/s)	coke's chemical reaction rate constant with i -th gaseous species
$K_{S,eff}$ ($\text{W}/\text{m}\cdot\text{K}$)	solid phase effective thermal conductivity
Pr	Prandtl number
Re	Reynolds number
r_0 (m)	initial radius of particle
r (m)	radius of particle
R_j ($\text{mol}/\text{m}^3\cdot\text{s}$)	reaction rate of j -th gas–gas reaction
R_k ($\text{mol}/\text{m}^3\cdot\text{s}$)	reaction rate of k -th gas–solid reaction
$SOURCE_g$ ($\text{J}/\text{m}^3\cdot\text{s}$)	gas phase energy equation source term
$SOURCE_i$ ($\text{kg}/\text{m}^3\cdot\text{s}$)	i -th gaseous species transportation equation's source term
$SOURCE_{mass-g}$ ($\text{kg}/\text{m}^3\cdot\text{s}$)	mass of the gas produced by gas phase reaction
$SOURCE_{mass-s}$ ($\text{kg}/\text{m}^3\cdot\text{s}$)	mass of the gas produced by gas–solid phase reaction
$SOURCE_{momentum}$ ($\text{kg}/\text{m}^2\cdot\text{s}^2$)	momentum equation source term
$SOURCE_s$ ($\text{J}/\text{m}^3\cdot\text{s}$)	solid phase energy equation source term
t (s)	time
T (K)	temperature
T_g (K)	gas phase temperature
T_s (K)	solid phase temperature
V (m/s)	gas flow rate in material layer
W	resistance coefficient of iron oxides reduction
Y_i	i -th gaseous species mass fraction
X	shape factor
ϵ	blackness of gas–solid radiation system
ϵ_s	blackness of solid phase
ϵ_g	blackness of gas phase
ϵ	porosity
ρ_g (kg/m^3)	gas phase density
ρ_s (kg/m^3)	solid material density
σ	Stefan–Boltzmann constant
α	heat distribution coefficient

λ_g (W/(m·K))	gas thermal conductivity
λ_s (W/(m·K))	gas thermal conductivity
μ (kg/m·s)	gas dynamic viscosity

References

- Wang, Y.; Zhang, J.; Liu, Z.; Du, C. Recent Advances and Research Status in Energy Conservation of Iron Ore Sintering in China. *JOM* **2017**, *69*, 2404–2411. [\[CrossRef\]](#)
- Chen, L.; Feng, H.; Xie, Z. Generalized Thermodynamic Optimization for Iron and Steel Production Processes: Theoretical Exploration and Application Cases. *Entropy* **2016**, *18*, 353. [\[CrossRef\]](#)
- Suopajarvi, H.; Kemppainen, A.; Haapakangas, J.; Fabritius, T. Extensive Review of the Opportunities to Use Biomass-Based Fuels in Iron and Steelmaking Processes. *J. Clean. Prod.* **2017**, *148*, 709–734. [\[CrossRef\]](#)
- Cheng, Z.; Tan, Z.; Guo, Z.; Yang, J.; Wang, Q. Recent Progress in Sustainable and Energy-Efficient Technologies for Sinter Production in the Iron and Steel Industry. *Renew. Sustain. Energy Rev.* **2020**, *131*, 110034. [\[CrossRef\]](#)
- Kieckhefen, P.; Pietsch, S.; Dosta, M.; Heinrich, S. Possibilities and Limits of Computational Fluid Dynamics–Discrete Element Method Simulations in Process Engineering: A Review of Recent Advancements and Future Trends. *Annu. Rev. Chem. Biomol. Eng.* **2020**, *11*, 397–422. [\[CrossRef\]](#)
- Abreu, G.C.; de Carvalho, J.A., Jr.; da Silva, B.E.C.; Pedrini, R.H. Operational and Environmental Assessment on the Use of Charcoal in Iron Ore Sinter Production. *J. Clean. Prod.* **2015**, *101*, 387–394. [\[CrossRef\]](#)
- Qian, L.; Zhang, Y.; Long, H.; Meng, Q.; Li, N. Effect of Gangue Composition on Assimilation Characteristic of Iron Ore in the Sintering Process. *Ironmak. Steelmak.* **2020**, *47*, 973–979. [\[CrossRef\]](#)
- Upadhyaya, G.S. Some Issues in Sintering Science and Technology. *Mater. Chem. Phys.* **2001**, *67*, 1–5. [\[CrossRef\]](#)
- Park, J.; Lee, S.; Park, J.Y. Review of Computational Fluid Dynamics Modeling of Iron Sintering Process. *J. Mech. Sci. Technol.* **2022**, *36*, 4501–4508. [\[CrossRef\]](#)
- Yan, F.; Zhang, X.; Yang, C.; Hu, B.; Qian, W.; Song, Z. Data-Driven Modeling Methods in Sintering Process: Current Research Status and Perspectives. *Can. J. Chem. Eng.* **2022**, *101*, 4506–4522. [\[CrossRef\]](#)
- Cook, P.S.; Murphy, A.B. Simulation of Melt Pool Behaviour during Additive Manufacturing: Underlying Physics and Progress. *Addit. Manuf.* **2020**, *31*, 100909. [\[CrossRef\]](#)
- Saidi, M.S.; Hajaligol, M.R.; Mhaisekar, A.; Subbiah, M. A 3D Modeling of Static and Forward Smoldering Combustion in a Packed Bed of Materials. *Appl. Math. Model.* **2007**, *31*, 1970–1996. [\[CrossRef\]](#)
- Hekkala, L.; Fabritius, T.; Härkki, J. Mathematical Model of Heat and Mass Transfer in the Steel Belt Sintering Process. In Proceedings of the Tenth International Ferroalloys Congress, Cape Town, South Africa, 1–4 February 2004; Volume 1, p. 4.
- Pahlevaninezhad, M.; Emami, M.D.; Panjepour, M. The Effects of Kinetic Parameters on Combustion Characteristics in a Sintering Bed. *Energy* **2014**, *73*, 160–176. [\[CrossRef\]](#)
- Fatehi, M.; Kaviany, M. Role of Gas-Phase Reaction and Gas-Solid Thermal Nonequilibrium in Reverse Combustion. *Int. J. Heat Mass Transf.* **1997**, *40*, 2607–2620. [\[CrossRef\]](#)
- Wang, J.; Ma, P.; Meng, H.; Cheng, F.; Zhou, H. Investigation on the Evolution Characteristics of Bed Porous Structure during Iron Ore Sintering. *Particuology* **2023**, *74*, 35–47. [\[CrossRef\]](#)
- Nyembwe, A.M.; Cromarty, R.D.; Garbers-Craig, A.M. Simulation of the Pressure Drop across Granulated Mixtures Using a Coupled DEM–CFD Model. *Adv. Powder Technol.* **2019**, *30*, 85–97. [\[CrossRef\]](#)
- Ma, W.; Ma, C.; Liu, X.; Gu, T.; Thengane, S.K.; Bourtsalas, A.; Chen, G. Nox Formation in Fixed-Bed Biomass Combustion: Chemistry and Modeling. *Fuel* **2021**, *290*, 119694. [\[CrossRef\]](#)
- Zhang, X.; Feng, P.; Xu, J.; Feng, L.; Qing, S. Numerical Research on Combining Flue Gas Recirculation Sintering and Fuel Layered Distribution Sintering in the Iron Ore Sintering Process. *Energy* **2020**, *192*, 116660. [\[CrossRef\]](#)
- Fu, J.; Cai, J. Study of Heat Transfer and the Hydrodynamic Performance of Gas–Solid Heat Transfer in a Vertical Sinter Cooling Bed Using the CFD-Taguchi-Grey Relational Analysis Method. *Energies* **2020**, *13*, 2225. [\[CrossRef\]](#)
- Zhou, H.; Wang, J.; Ma, P.; Meng, H.; Cheng, F.; Luo, J. Influence of Quick Lime on Pore Characteristics of High-Temperature Zone in Iron Ore Sinter Based on XCT Technology. *J. Mater. Res. Technol.* **2021**, *15*, 4475–4486. [\[CrossRef\]](#)
- Banjare, Y.P.; Sahoo, R.K.; Sarangi, S.K. CFD Simulation of a Gifford–McMahon Type Pulse Tube Refrigerator. *Int. J. Therm. Sci.* **2009**, *48*, 2280–2287. [\[CrossRef\]](#)
- Pu, Z.; Zhou, F.; Sun, Y.; Zhang, M.; Li, B. Modelling and Numerical Simulation of Isothermal Oxidation of an Individual Magnetite Pellet Based on Computational Fluid Dynamics. *J. Iron Steel Res. Int.* **2021**, *28*, 799–808. [\[CrossRef\]](#)
- Venkataramana, R.; Gupta, S.S.; Kapur, P.C.; Ramachandran, N. Mathematical Modelling and Simulation of the Iron Ore Sintering Process. *Tata Search* **1998**, *5*, 25–30.
- Hayashi, N.; Komarov, S.V.; Kasai, E. Heat Transfer Analysis of the Mosaic Embedding Iron Ore Sintering (MEBIOS) Process. *ISIJ Int.* **2009**, *49*, 681–686. [\[CrossRef\]](#)
- Huang, X.X.; Fan, X.H.; Chen, X.L.; Zhao, X.Z.; Gan, M. Optimisation Model of Fuel Distribution in Materials Bed of Iron Ore Sintering Process. *Ironmak. Steelmak.* **2019**, *46*, 649–655. [\[CrossRef\]](#)
- Shen, X.; Chen, L.; Xia, S.; Sun, F. Numerical Simulation and Analyses for Sinter Cooling Process with Convective and Radiative Heat Transfer. *Int. J. Energy Environ.* **2016**, *7*, 303.

28. Ljung, A.-L.; Lundström, T.S.; Tano, K. Simulation of Heat Transfer and Fluid Flow in a Porous Bed of Iron Ore Pellets during Up-Draught Drying. *Simulation* **2006**, *13*, 15.
29. Martin, H. Low Peclet Number Particle-to-Fluid Heat and Mass Transfer in Packed Beds. *Chem. Eng. Sci.* **1978**, *33*, 913–919. [[CrossRef](#)]
30. Abdelmotalib, H.M.; Youssef, M.A.M.; Hassan, A.A.; Youn, S.B.; Im, I.-T. Heat Transfer Process in Gas–Solid Fluidized Bed Combustors: A Review. *Int. J. Heat Mass Transf.* **2015**, *89*, 567–575. [[CrossRef](#)]
31. Dombrovskii, L.A. Approximate Methods for Calculating Radiation Heat Transfer in Dispersed Systems. *Therm. Eng.* **1996**, *43*, 235–243.
32. Wang, G.; Wen, Z.; Lou, G.; Dou, R.; Li, X.; Liu, X.; Su, F. Mathematical Modeling of and Parametric Studies on Flue Gas Recirculation Iron Ore Sintering. *Appl. Therm. Eng.* **2016**, *102*, 648–660. [[CrossRef](#)]
33. Jena, S.K.; Sahoo, H.; Rath, S.S.; Rao, D.S.; Das, S.K.; Das, B. Characterization and Processing of Iron Ore Slimes for Recovery of Iron Values. *Miner. Process Extr. Metall. Rev.* **2015**, *36*, 174–182. [[CrossRef](#)]
34. Zhao, J.P.; Loo, C.E.; Dukino, R.D. Modelling Fuel Combustion in Iron Ore Sintering. *Combust. Flame* **2015**, *162*, 1019–1034. [[CrossRef](#)]
35. Valipour, M.S.; Saboohi, Y. Modeling of Multiple Noncatalytic Gas–Solid Reactions in a Moving Bed of Porous Pellets Based on Finite Volume Method. *Heat Mass Transf.* **2007**, *43*, 881–894. [[CrossRef](#)]
36. Kong, W.; Fu, X.; Liu, Z.; Zhou, C.; Lei, J. A Facile Synthesis of Solid-Solid Phase Change Material for Thermal Energy Storage. *Appl. Therm. Eng.* **2017**, *117*, 622–628. [[CrossRef](#)]
37. Zhu, T.; Wang, X.; Li, C.; Xu, W.; Qin, S.; Song, J. Numerical Simulation of CO Emission in a Sintering Pot under Flue Gas Recirculation. *Chem. Eng. J.* **2023**, *452*, 139069. [[CrossRef](#)]
38. Jang, J.; Chiu, Y. 3-D Transient Conjugated Heat Transfer and Fluid Flow Analysis for the Cooling Process of Sintered Bed. *Appl. Therm. Eng.* **2009**, *29*, 2895–2903. [[CrossRef](#)]
39. Horio, M.; Muchi, I. Estimation of Heat Exchange Area in Sintering Beds Sustainable Scenario Development View Project Mass Localism View Project. *Tetsu Hagane* **1980**, *66*, 119–120. [[CrossRef](#)]
40. Nath, N.K.; Da Silva, A.J.; Chakraborti, N. Dynamic Process Modelling of Iron Ore Sintering. *Steel Res.* **1997**, *68*, 285–292. [[CrossRef](#)]
41. Liu, Y.; Wang, J.; Cheng, Z.; Yang, J.; Wang, Q. Experimental Investigation of Fluid Flow and Heat Transfer in a Randomly Packed Bed of Sinter Particles. *Int. J. Heat Mass Transf.* **2016**, *99*, 589–598. [[CrossRef](#)]
42. Yang, W.; Ryu, C.; Choi, S. Unsteady One-Dimensional Model for a Bed Combustion of Solid Fuels. *J. Power Energy* **2004**, *218*, 589–598. [[CrossRef](#)]
43. Castro, J.A.d.; Sasaki, Y.; Yagi, J. Three Dimensional Mathematical Model of the Iron Ore Sintering Process Based on Multiphase Theory. *Mater. Res.* **2012**, *15*, 848–858. [[CrossRef](#)]
44. De Castro, J.A.; Nath, N.; Franca, A.B.; Guilherme, V.S.; Sasaki, Y. Analysis by Multiphase Multicomponent Model of Iron Ore Sintering Based on Alternative Steelworks Gaseous Fuels. *Ironmak. Steelmak.* **2012**, *39*, 605–613. [[CrossRef](#)]
45. Aissa, A.; Abdelouahab, M.; Noureddine, A.; Elganaoui, M.; Pateyron, B. Ranz and Marshall Correlations Limits on Heat Flow between a Sphere and Its Surrounding Gas at High Temperature. *Therm. Sci.* **2015**, *19*, 1521–1528. [[CrossRef](#)]
46. Gao, Q.; Xie, J.; Zhang, Y.; Bao, L.; Zhou, H.; Ye, H. Mathematical Modeling of Natural Gas Injection in Iron Ore Sintering Process and Corresponding Environmental Assessment of CO₂ Mitigation. *J. Clean. Prod.* **2022**, *332*, 130009. [[CrossRef](#)]
47. Tan, P.; Neuschütz, D. CFD Modeling of Sintering Phenomena during Iron Ore Sintering. In Proceedings of the Multiphase Phenomena and CFD Modeling and Simulation in Materials Processes as Held at the 2004 TMS Annual Meeting, Charlotte, NC, USA, 14–18 March 2004; pp. 451–459.
48. Sun, C.; Ma, P.; Deng, J.; Bai, L.; Liao, Z.; Pei, Y.; Zhang, Q.; Xu, J. Intensive Reduction of Fuel Consumption in the Sintering Process of Double-Layered Fuel Segregation with Return Fines Embedding. *Fuel* **2023**, *332*, 125955. [[CrossRef](#)]
49. Zhou, M.; Zhou, H.; Ma, P.; Xu, J. Effect of Coke Rate and Basicity on Computed Tomography-Measured Pore Parameters and Effective Thermal Conductivity of Iron Ore Sinter. *J. Mater. Res. Technol.* **2019**, *8*, 6191–6201. [[CrossRef](#)]
50. Lafmejani, S.S.; Emami, M.D.; Panjepour, M.; Sohrabi, S. Two-Dimensional Axisymmetric Modeling of Combustion in an Iron Ore Sintering Bed. *Spec. Top. Rev. Porous Media Int. J.* **2013**, *4*, 299–313. [[CrossRef](#)]
51. Go, K.S.; Son, S.R.; Kim, S.D. Reaction Kinetics of Reduction and Oxidation of Metal Oxides for Hydrogen Production. *Int. J. Hydrogen Energy* **2008**, *33*, 5986–5995. [[CrossRef](#)]
52. Schneiderbauer, S.; Kinaci, M.E.; Hauzenberger, F. Computational Fluid Dynamics Simulation of Iron Ore Reduction in Industrial-Scale Fluidized Beds. *Steel Res. Int.* **2020**, *91*, 2000232. [[CrossRef](#)]
53. Tso, C.Y.; Chao, C.Y.H. Study of Enthalpy of Evaporation, Saturated Vapor Pressure and Evaporation Rate of Aqueous Nanofluids. *Int. J. Heat Mass Transf.* **2015**, *84*, 931–941. [[CrossRef](#)]
54. Gao, Q.; Bao, L.; Zhu, P.; Jiang, X.; Zheng, H.; Shen, F. Mathematical Simulation of Iron Ore Fines Sintering Process with Solid Fuel Segregation Distribution and Corresponding Heat Pattern Study. *Metals* **2022**, *12*, 2126. [[CrossRef](#)]
55. Hou, P.; Choi, S.; Yang, W.; Choi, E.; Kang, H. Application of Intra-Particle Combustion Model for Iron Ore Sintering Bed. *Mater. Sci. Appl.* **2011**, *2*, 370. [[CrossRef](#)]
56. Lee, W.H. A Pressure Iteration Scheme for Two-Phase Flow Modeling. *Multiph. Transp. Fundam. React. SAFETY Appl.* **1980**, 407–432.

57. Chao, L.; Zhang, Y.; Shi, Y.; Xing, H.; Kang, Y.; Li, J. Numerical Simulation of Sintering Based on Biomass Fuel. *Ironmak. Steelmak.* **2018**, *45*, 700–707. [[CrossRef](#)]
58. Tukamoto, T.; Simada, S.; Taguchi, T.; Higuchi, J. Analysis of Sintering Process by the Mathematical Model. *Tetsu Hagane* **1970**, *56*, 661–670. [[CrossRef](#)] [[PubMed](#)]
59. Bross, P.; Exner, H.E. Computer Simulation of Sintering Processes. *Acta Metall.* **1979**, *27*, 1013–1020. [[CrossRef](#)]
60. Asai, S.; Muchi, I. Theoretical Analysis on the Effective Distribution Coefficient for Solidification Accompanied with Liquid and Solid Region Cases Taking Account of Diffusion in Solid Phase or Diffusion Boundary Layer. *Tetsu Hagane* **1979**, *65*, 203–211. [[CrossRef](#)]
61. Higuchi, J.; Iwao, M. Mathematical Model of Sintering Bed. *Tetsu Hagane* **1967**, *53*, 1171–1173. [[CrossRef](#)]
62. Liu, Y.; Yang, J.; Wang, J.; Cheng, Z.; Wang, Q. Energy and Exergy Analysis for Waste Heat Cascade Utilization in Sinter Cooling Bed. *Energy* **2014**, *67*, 370–380. [[CrossRef](#)]
63. Toda, H.; Kato, K. Theoretical Investigation of Sintering Process. *Trans. Iron Steel Inst. Jpn.* **1984**, *24*, 178–186. [[CrossRef](#)]
64. Kasai, E.; Yagi, J.I.; Omori, Y. Mathematical Modeling of Sintering Process Considering Influence of Changes in Void Fraction and Apparent Particle Size in the Bed on Pressure Drop. *Tetsu Hagane* **1984**, *70*, 1567–1574. [[CrossRef](#)] [[PubMed](#)]
65. Kawaguchi, T.; Sato, S.; Takata, K. Development and Application of an Integrated Simulation Model for Iron Ore Sintering. *Tetsu Hagane* **1987**, *73*, 138–145.
66. Jianming, L.; Zhaoxiang, Y. Study on Mathematical Model of Sintering Process. *Sinter. Pelletizing* **1990**, *15*, 1–9.
67. Yamaoka, H.; Kawaguchi, T. Development of a 3-D Sinter Process Mathematical Simulation Model. *ISIJ Int.* **2005**, *45*, 522–531. [[CrossRef](#)]
68. Kawaguchi, T.; Yamaoka, H. Development of a 3 Dimensional Mathematical Simulation Model for Iron Ore Sintering Process. *Tetsu Hagane* **2006**, *92*, 769–778. [[CrossRef](#)]
69. Zhang, B.; Zhou, J.; Li, M. Prediction of Sinter Yield and Strength in Iron Ore Sintering Process by Numerical Simulation. *Appl. Therm. Eng.* **2018**, *131*, 70–79. [[CrossRef](#)]
70. Mitterlehner, J.; Löffler, G.; Winter, F.; Hofbauer, H.; Schmid, H.; Zwittag, E.; TH, B.; Pammer, O.; Stiasny, H. Modeling and Simulation of Heat Front Propagation in the Iron Ore Sintering Process. *ISIJ Int.* **2004**, *44*, 11–20. [[CrossRef](#)]
71. Yang, W.; Ryu, C.; Choi, S.; Choi, E.; Lee, D.; Huh, W. Modeling of Combustion and Heat Transfer in an Iron Ore Sintering Bed with Considerations of Multiple Solid Phases. *ISIJ Int.* **2004**, *44*, 492–499. [[CrossRef](#)]
72. Zhang, X.; Chen, Z.; Zhang, J.; Ding, P.; Zhou, J. Simulation and Optimization of Waste Heat Recovery in Sinter Cooling Process. *Appl. Therm. Eng.* **2013**, *54*, 7–15. [[CrossRef](#)]
73. Zhou, H.; Zhou, M.; Cheng, M.; Guo, W.; Cen, K. Experimental Study and X-Ray Microtomography Based CFD Simulation for the Characterization of Pressure Drop in Sinter Bed. *Appl. Therm. Eng.* **2017**, *112*, 811–819. [[CrossRef](#)]
74. Zhou, H.; Zhou, M.; Cheng, M.; Guo, X.; Li, Y.; Ma, P.; Cen, K. High Resolution X-Ray Microtomography for the Characterization of Pore Structure and Effective Thermal Conductivity of Iron Ore Sinter. *Appl. Therm. Eng.* **2017**, *127*, 508–516. [[CrossRef](#)]
75. Zhou, H.; Meng, H.; Ma, P.; Wang, J.; Cheng, F.; Fang, H. Experimental Investigation on the Effect of Granulation Moisture on the Flame Front Propagation and Pore Structure in the High-Temperature Zone of the Sinter Bed. *Powder Technol.* **2022**, *396*, 663–672. [[CrossRef](#)]
76. Zhang, B.; Zhou, J.; Li, M.; Li, Y. Modeling and Simulation of Iron Ore Sintering Process with Consideration of Granule Growth. *ISIJ Int.* **2018**, *58*, 17–24. [[CrossRef](#)]
77. Gauna, E.A.; Zhao, Y. Numerical Simulation of Heat Transfer in Porous Metals for Cooling Applications. *Metall. Mater. Trans. B* **2017**, *48*, 1925–1932. [[CrossRef](#)]
78. Liu, Y.; Wang, J.; Yuan, X.; Yang, J.; Wang, Q.W. Numerical Investigation of Sinter Cooling Process in Sinter Cooler. In Proceedings of the AIP Conference Proceedings, American Institute of Physics, Antalya, Turkey, 24–28 April 2013; Volume 1547, pp. 788–795.
79. Feng, J.; Dong, H.; Gao, J.; Li, H.; Liu, J. Numerical Investigation of Gas-Solid Heat Transfer Process in Vertical Tank for Sinter Waste Heat Recovery. *Appl. Therm. Eng.* **2016**, *107*, 135–143. [[CrossRef](#)]
80. Cheng, Z.; Wang, J.; Wei, S.; Guo, Z.; Yang, J.; Wang, Q. Optimization of Gaseous Fuel Injection for Saving Energy Consumption and Improving Imbalance of Heat Distribution in Iron Ore Sintering. *Appl. Energy* **2017**, *207*, 230–242. [[CrossRef](#)]
81. Cheng, Z.; Wei, S.; Guo, Z.; Yang, J.; Wang, Q. Improvement of Heat Pattern and Sinter Strength at High Charcoal Proportion by Applying Ultra-Lean Gaseous Fuel Injection in Iron Ore Sintering Process. *J. Clean. Prod.* **2017**, *161*, 1374–1384. [[CrossRef](#)]
82. Cheng, Z.; Fu, P.; Guo, Z.; Yang, J.; Wang, Q. CFD Prediction of Heat/Mass Transfer in Multi-Layer Sintering Process Assisted with Gaseous Fuel Injection. *Int. Commun. Heat Mass Transf.* **2021**, *128*, 105654. [[CrossRef](#)]
83. Huang, X.; Fan, X.; Ji, Z.; Gan, M.; Chen, X.; Zhao, Y.; Jiang, T. Investigation into the Characteristics of H₂-Rich Gas Injection over Iron Ore Sintering Process: Experiment and Modelling. *Appl. Therm. Eng.* **2019**, *157*, 113709. [[CrossRef](#)]
84. Tsioutsios, N.; Weiss, C.; Rieger, J.; Schuster, E.; Geier, B. Flame Front Progress in Gas Assisted Iron Ore Sintering. *Appl. Therm. Eng.* **2020**, *165*, 114554. [[CrossRef](#)]
85. Nath, N.K.; Mitra, K. Mathematical Modeling and Optimization of Two-Layer Sintering Process for Sinter Quality and Fuel Efficiency Using Genetic Algorithm. *Mater. Manuf. Process* **2005**, *20*, 335–349. [[CrossRef](#)]
86. Giri, B.K.; Roy, G.G. Mathematical Modelling of Iron Ore Sintering Process Using Genetic Algorithm. *Ironmak. Steelmak.* **2012**, *39*, 59–66. [[CrossRef](#)]

87. Mallick, A.; Dhara, S.; Rath, S. Application of Machine Learning Algorithms for Prediction of Sinter Machine Productivity. *Mach. Learn. Appl.* **2021**, *6*, 100186. [[CrossRef](#)]
88. Ramos, M.V.; Kasai, E.; Kano, J.; Nakamura, T. Numerical Simulation Model of the Iron Ore Sintering Process Directly Describing the Agglomeration Phenomenon of Granules in the Packed Bed. *ISIJ Int.* **2000**, *40*, 448–454. [[CrossRef](#)]
89. Wei, H.; Nie, H.; Li, Y.; Saxén, H.; He, Z.; Yu, Y. Measurement and Simulation Validation of DEM Parameters of Pellet, Sinter and Coke Particles. *Powder Technol.* **2020**, *364*, 593–603. [[CrossRef](#)]

Disclaimer/Publisher’s Note: The statements, opinions and data contained in all publications are solely those of the individual author(s) and contributor(s) and not of MDPI and/or the editor(s). MDPI and/or the editor(s) disclaim responsibility for any injury to people or property resulting from any ideas, methods, instructions or products referred to in the content.